Flexible surface acoustic wave resonators built on disposable plastic film for electronics and lab-on-a-chip applications

Hao Jin,[1] Jian Zhou,[1] Xingli He,[1] Wenbo Wang,[1] Hongwei Guo,[1] Shurong Dong,[1] Demiao Wang,[1] Yang Xu,[1]* Junfeng Geng,[2] Jikui Luo[1,2,]* and W.I.Milne[3]

[1]Department of Information Science and Electronic Engineering, Zhejiang University, Hangzhou 310027, P. R. China

[2] Institute of Renewable Energy and Environmental Technologies, University of Bolton, Bolton BL3 5AB, U.K

[3] Department of Engineering, University of Cambridge, Cambridge, CB3 0HE U.K.

*Corresponding authors. E-mails: yangxu-isee@zju.edu.cn; J.Luo@bolton.ac.uk

Flexible electronics are a very attractive and promising technology for a number of applications. Various types of flexible electronic devices have been developed, but there has been limited research on flexible electromechanical systems (MEMS). Surface acoustic wave (SAW) devices are not only an essential electronic device, but can also act as the building blocks for sensors and MEMS. In this paper, we report a method of making flexible SAW devices using ZnO nanocrystals deposited on a cheap, bendable and disposable plastic film. The flexible SAW devices exhibit two wave modes for the Rayleigh wave and Lamb wave with resonant frequencies of up to 198.1 MHz and 447.0 MHz respectively, and transmission signal amplitudes of up to 18 dB. These flexible SAW devices have a high temperature coefficient of frequency, and are thus useful as sensitive temperature sensors. Moreover, strong acoustic streaming with a velocity of up to 3.4 cm/s and particle concentration using the SAW have been achieved, demonstrating the great potential for applications in electronics and MEMS.

Flexible electronic devices such as field effect transistors and its associated integrated circuits[1,2] are central to many applications such as displays[3,4], eyeball cameras[5], memory[6], lithium-ion batteries[7]. Flexible microelectromechanical systems (MEMS) add to the flexible electronic devices family, and have important and widespread applications. Various MEMS devices and systems have been developed such as the micro-machined infrared bolometer[8], piezoelectric actuators[9], thin film bulk acoustic wave resonators[10], piezoelectric pressure sensors[11], and micro-fluidics[12]. Surface acoustic wave (SAW) devices are crucial for the development of many MEMS devices and systems as they are the fundamental building blocks for microsensors and microsystems[13-24]. However, the lack of an effective approach for the manufacture of flexible and high performance SAW devices has been the major obstacle to the exploitation of many proposed flexible electronic applications for sensors and MEMS, especially in microfluidics and lab-on-a-chip.

SAW devices have a very wide range of applications including their use in radio-frequency communication as filters, frequency duplexers and RF tags (RFIDs), in biochemical sensing, drug development, healthcare, medical and life sciences as micro-sensors for measuring physical parameters and detecting biochemical substances[13-19], and micro-actuators for microfluidics[21,22] as well as for lab-on-a-chip applications[22-24]. SAW devices are normally made on piezoelectric (PE) substrates such as $LiNbO_3$, or by PE thin films such as zinc oxide (ZnO) or aluminum nitride (AlN) deposited on rigid substrates such as silicon (Si) or sapphire. However, it would be a huge benefit if a SAW device can be constructed at a low cost on a cheap and flexible substrate such as on plastic films, which may be either disposable or recyclable. But so far there is no report of such SAW devices because of the difficulties in achieving the growth of high-quality PE films with large areas on a flexible substrate[25]. It is especially difficult to obtain highly c-axis oriented, low surface roughness PE films with a good piezoelectric constant. The following factors may be particularly responsible for the current situation: (1) Most flexible substrates are amorphous, hence they do not match the

lattices of the required PE crystals; (2) The large differences in the thermal expansion coefficients between the substrates and the PE films cause serious problems in the film deposition[26]; (3) SAW devices generally demand thick PE layers (the thickness must be larger than 10% of the SAW wavelength), which makes film growth and fabrication processing difficult. Here we report a method of making flexible SAW devices using ZnO nanorods deposited on a polyimide (PI) substrate – a cheap, bendable and disposable plastic film, and their excellent performance of transmission, strong acoustic streaming and particle sorting etc, demonstrating their potential applications in flexible electronic devices, sensing, microfluidics and lab-on-a-chip.

Results

Nanocrystalline ZnO piezoelectric films. To make the flexible devices, a Kapton® polyimide (PI) film 100H (Toray, Dupont, thickness 100 μm) was chosen as the substrate because of its excellent flexibility, good mechanical and electrical properties, its chemical stability, and its wide operating temperature range (−269 to 400 °C)[27]. Figure 1 shows a schematic drawing of the structure of the device (Figure 1a), a microscopic top view of the interdigitated transducer (IDT) electrode (Figure 1b), and photographs of the fabricated devices on the PI film (Figure 1c and 1d). In this work, three different groups of devices, denoted as A, B and C, have been fabricated using conventional ultraviolet photolithography techniques and a simple lift-off process. In group A, the thickness of the ZnO films was fixed at 4 μm, while the acoustic wave wavelength, λ, was varied to be λ = 10 μm, 12 μm, 16 μm, 20 μm, 24 μm, and 32 μm, respectively, by changing the IDT spacing. In group B and C, the wavelengths were fixed at 16 μm and 12 μm respectively, while the thickness of the ZnO films was varied from 1.7 μm to 4 μm. The detailed parameters of these three groups of devices are summarized in Tables S1 and S2 in the Supplementary Information (*SI*).

The ZnO films were made up of vertically-aligned ZnO nanocrystals deposited on the PI substrates using a home-made direct-current magnetron sputtering system. A water-cooled zinc target of purity 99.999% was employed for the deposition under a flow of O_2/Ar mixture with a deposition pressure of 2 Pa (see *SI* for details). Figure 2a shows a scanning electron microscope (SEM) photo of a 4 μm thick ZnO thin film as an example. It can be seen that the ZnO film consists of highly-oriented columnar nanograins perpendicular to the substrate, a growth result that is similar to what has been previously achieved on Si substrates[28,29]. X-ray diffraction (XRD) characterization reveals that the (002) ZnO crystal orientation dominates the crystal orientation (Figure 2b). The full-width at half-maximum (FWHM) of the XRD peak is 0.152°, smaller than most of those obtained from similar thin films deposited on rigid substrates.

The mean crystallite grain size, *D*, was estimated to be ~72.3 nm using the Debye–Scherrer formula[30] (see *SI* for details), similar to the ZnO nanorods previously deposited on solid substrates[31]. The biaxial stress which is less than 100 MPa for all the films deposited was estimated from the lattice constant obtained from the XRD patterns. This enables the films to be directly used for the fabrication of the SAW devices without any thermal annealing to remove the stress in the films. Figure 2c and 2d show the morphology and surface roughness of the films measured by atomic force microscopy (AFM). Here the root mean square (RMS) roughness was estimated to be ~9 nm over an area of 4 × 4 μm^2, comparable to those obtained from the films deposited on solid substrates[32,33], suggesting that the films are sufficiently smooth for the fabrication of SAW devices.

SAW transmission characteristics. The transmissions (S_{21}) and reflections (S_{11}) of all the group A devices exhibit two well-defined resonant peaks (Figure 3), the zero mode resonant peak with a frequency, f_0, of 34.4, 56.4, 75.0, 101.5, 161.0 and 198.1 MHz respectively, and the first mode resonant peak with a frequency, f_1, varying in the range from 158.5 to 447.0

MHz, both corresponding to the respective wavelength of 32, 24, 20, 16, 12 or 10 μm (See Table S1 in *SI*). A large transmission signal amplitude of up to ~18 dB was obtained for both the wave modes, indicating that the performance of the fabricated flexible SAW devices is sufficient for electronic and communication applications. It was also observed that in most fabricated devices, the signal amplitude of the first resonant mode is higher than that of the zero resonant one, suggesting that the first mode resonance can be better used for high frequency applications. Moreover, our finite element analysis (FEA) (see *SI* for details) has revealed the nature of the two resonant modes: the zero mode resonance corresponds to the Rayleigh wave, and the first mode to the Lamb wave.

To understand more about the experimental results, we have performed simulations and theoretical[34] calculations on the resonant frequencies and phase velocities (see *SI* for details). Figure 4a shows an example for comparison between the experimental spectrum (S_{11}) and the simulated one from the FEA. It can be seen that the two spectra are consistent with one another though the amplitude of the experimental one is much smaller due to the polycrystalline nature of the actual film whereas a single crystal structure is assumed for the simulation and theoretical calculations. Likewise, Figure 4b illustrates the results of the experimental phase velocities (v_{pi}) and the simulated and calculated ones for both the Rayleigh and the Lamb wave modes. Here the velocity is determined from $v_{pi} = \lambda_i f_i$ (i = 0 or 1, corresponding to the Rayleigh or the Lamb wave) at the fixed wavelengths of λ_i = 32, 24, 20, 16, 12 and 10 μm, respectively. Clearly, v_{p0} increases from 1101 to 1981 m/s, and v_{p1} decreases from 5072 m/s to 4470 m/s with decrease in wavelength. The theoretical calculations of the phase velocities agree well with the experimental and the simulated ones.

It is noted that for a layered structure, the phase velocity is influenced by the intrinsic properties of the piezoelectric layer and the substrate. In an ideal (002) ZnO layer, the theoretical phase velocity limit of the Rayleigh mode would be ~2650 m/s, while this velocity in polyimide is much smaller and is estimated to be ~754 m/s (see *SI* for details). In this case,

when the wavelength is reduced, the acoustic waves will be more confined in the ZnO layer. At the short wavelength of λ = 10 μm, which is 2.5 times the ZnO film thickness, the phase velocity (~1981 m/s in this case) already accounts for ~75% of the theoretical limit of the ZnO, demonstrating the excellent properties of the deposited films and the SAW devices fabricated. Since the phase velocity in ZnO is much higher than that in polyimide, the Lamb waves are expected to co-exist in this layered structure[35], as has been confirmed by our experiments and simulation.

In addition to the materials used to make the layered structure, it should be noted that the ZnO film thickness has a strong effect on both the resonant frequency and the phase velocity of the Rayleigh and Lamb waves. This thickness effect was tested by fixing the wavelength at either λ = 16 μm or 12 μm (Figure 5, and Table S2 in *SI*). It was found that both the resonant frequency (f_0) and phase velocity (v_{p0}) of the Rayleigh wave increased with increase in film thickness. However, for the Lamb wave, the film thickness showed an opposite effect, i.e., the increase in film thickness reduces the values of f_1 and v_{p1}. For comparison, the simulated results are shown in Figure 6. It can be seen that at both scanned wavelengths, v_{p1} approaches its limit of ~5510 m/s in an extremely thin ZnO layer, and that the change of frequencies from device to device is indeed caused by the variation of the ZnO thickness and wavelength.

Based on the above results, we conclude that a Rayleigh wave resonant frequency f_0 of 198.1 MHz, v_p of 1981 m/s and K^2 of 1.05 %, and a Lamb wave resonant frequency f_1 of 447 MHz, v_{p1} of 4470 m/s and K^2 of 0.8 % have been obtained in this work (See *SI* for details). The slightly larger values of the simulated results compared to the experimental data as shown in figure 6b are probably due to the use of ideal material constants for the simulation, which are certainly better than the actual ones for the ZnO film and the polyimide as these layers may have defects and a damaged surface caused by ion bombardment during the deposition. However, the overall excellent performance, especially the high resonant frequencies and large transmission signals of both the Rayleigh and Lamb waves, demonstrate that our

flexible SAW devices have great potential for electronics, sensors and lab-on-a-chip applications.

Flexible SAW temperature sensor. It is well known that SAW devices are extremely useful in the development of sensors owing to their high sensitivity[17]. To this end, SAW devices have been utilized as wireless sensors for monitoring changes of various physical parameters such as temperature[13] and pressure[14, 36] because of their structural simplicity and easy operation. Flexible SAW devices can play an important role in this respect owing to the thin film structure and low cost etc. Furthermore SAW devices can be used for microfluidics and lab-on-a-chip[37] owing to their large actuation force, high flow velocity and non-moving component characteristics. In fact, they have been used for biodetection and liquid pumping and mixing. If flexible SAW devices can be proven to be useful for high performance sensors and microfluidics, this will open the door for widespread applications for inexpensive and disposable lab-on-a-chip applications for healthcare, medical research and biotechnologies. As examples, we have conducted experiments on temperature sensing, acoustic-induced streaming and particle concentration and sorting using the flexible SAW devices developed in this work to verify their suitability for these applications.

The resonant frequencies of the Rayleigh and Lamb waves of the flexible SAW devices have been obtained as a function of temperature with the results shown in Figure 7. The frequencies measured for both the wave modes decrease linearly with increase of temperature, which is the same trend as observed from other SAW devices built on rigid substrates[37,38]. The temperature coefficients of frequency (TCF), defined as $\Delta f/\Delta T f_0$, are ~442 and ~245 ppm/K for the zero and first modes respectively, and are almost constant for devices with different wavelengths and from different substrates. Both of these values are much larger than the TCF of the Rayleigh wave from the rigid ZnO/Si (~67 ppm/K)[38] and the bulk $LiNbO_3$ (70-80 ppm/K)[37] SAW devices. This is attributed to the much larger thermal expansion coefficient

of the polyimide substrate (20 ppm/K, Dupont database) than that of the Si substrate (~3.0 ppm/K). The excellent linearity and large TCFs of the flexible SAW devices are better than those reported for rigid SAW devices for the development of sensitive temperature sensors for measurements, calibrations or as a reference for other sensing systems.

Flexible SAW Microfluidics. When a liquid droplet is located in the path of a surface acoustic wave, the SAW will interact with the liquid and the acoustic energy will be coupled into the liquid, inducing acoustic streaming as schematically shown in Figure 8a. This has been utilized for pumping[22], mixing[19], atomization[39], particle concentration and sorting[40,41]. We found that the flexible SAW devices can deliver the same functions as those built on solid and unbendable substrates. Figure 8b is a snap shot of the acoustic streaming inside a 2 μL droplet induced by the Rayleigh wave from a flexible SAW device, showing a stable streaming with a double vortex pattern similar to those obtained from the SAW devices on stiff substrates[21]. The acoustic streaming can be viewed from the Movie in the Supplementary Information section. The SAW devices used for this experiment have a resonant frequency of f_0 = 161.1 MHz (Device A2). Figure 8c shows the streaming velocities measured at the centre of the droplets of different sizes as a function of RF signal voltage. The streaming velocities were found to increase almost linearly with the increase of RF signal voltage applied to the IDT electrode. These velocities also increase with the increase in droplet size, and reach 3.4 cm/s at a signal voltage of 9.5 V for a 10 μL droplet. Although the streaming velocities are lower than those of SAW devices on rigid substrates[40], it is more than enough for flexible SAW devices to be used in most microfluidic applications.

The flexible SAW devices have also been tested for the ability to perform particle concentration and sorting functions, one of many lab-on-a-chip applications in biotechnology and medical science. Here the droplet containing TiO_2 nano-particles is positioned off the central line of the wave path, which allows the SAW to induce a circulating streaming pattern,

generating a shear force which pushes particles towards the center of the droplet[40] as shown in Figure 8d. Figure 8e, 8f and 8g show the sequence of the particle concentration under a SAW. Uniformly distributed nano-particles are moved towards the centre of the droplet after a RF signal with a peak-to-peak voltage of 35V is applied to the IDT electrode. The nano-particles were concentrated in the centre of the droplet after ~70 seconds. The results show that the flexible SAW devices can indeed be used for microfluidics and lab-on-chip applications with similar excellent performance to those made on bulk PE substrates[40] or on PE films deposited on rigid substrates[21, 39,41].

In summary, ZnO piezoelectric thin films have been deposited on flexible polyimide substrates at low temperature by reactive magnetron sputtering. The ZnO thin films have (002) oriented, columnar grains with small surface roughness. Flexible ZnO/polyimide SAW devices have been fabricated. All the flexible SAW devices showed two resonant modes: the Rayleigh wave and Lamb wave with a resonant frequency and coupling coefficient of 198.1 MHz and 1.05 %, and of 447 MHz and 0.8 % respectively. Both the wave modes have a much larger TCF than those built on rigid substrates, hence are better for high sensitivity temperature sensors. Furthermore, strong acoustic streaming with a velocity of up to 3.4 cm s^{-1} and particle concentration using the SAW devices have been achieved. The results are comparable to those obtained from SAW devices made on rigid substrates. All these results have clearly demonstrated that our flexible SAW devices have great potential for applications in electronics and microsystems.

Methods

ZnO deposition on polymer substrates. ZnO thin films were deposited on the polymer substrates (Kapton® polyimide film 100H) using a direct-current (DC) magnetron sputtering system built in our laboratory. The base pressure of the chamber was 1×10^{-4} Pa before deposition. A water-cooled zinc target of purity 99.999% with a diameter of 100 mm was

used for the deposition of the ZnO films. The distance between the target and the substrate was fixed at 70 mm. The deposition conditions are as follows: O_2/Ar mixture gas has a ratio of 50/100 (sccm); the deposition pressure is 2 Pa; the DC sputtering power is 200 W; the substrate temperature is fixed at 100 °C, and the bias voltage is -75 V.

Crystal structure characterization. The crystalline structure of the ZnO films was analyzed using X-ray diffraction (XRD) (Panalytical Empyrean) with Cu- K_α radiation (λ = 0.154 nm) at 40 keV and 40 mA. The diffraction patterns were obtained in the 2θ mode with a scan range of 2θ = 20°~70°. For cross-sectional structural analysis, a scanning electron microscope (SEM) (Hitachi S-4800) was used with an accelerating voltage of 3 keV. The roughness of the film surfaces was investigated by atomic force microscopy (AFM) (SPI-3800N, Seiko Co.) under a tapping mode at 300 kHz.

SAW device fabrication and characterization. For all the SAW devices, an 80-100 nm thick Al layer was used for making the interdigitated transducer electrodes that have 20 or 50 pairs of fingers. The distance between the two IDT transducers was 80 λ, where the wavelength λ was determined by the IDT pitch. A reflection grating was used to enhance the strength of the standing wave. The S-parameters were measured using an Agilent E5071C network analyzer.

SAW microfluidics and particle concentration characterisation. For microfluidic tests, a RF signal from a signal generator (SP2410, made in China) was amplified by a RF power amplifier to obtain an RF signal with up to 50V peak to peak amplitude before being fed into the IDTs. Black ink was dissolved into DI water for streaming experiments. Water droplets with different sizes were obtained using a micropipette and the motion of black ink particles was captured by a high speed camera (Grasshopper 03K2C, with 200 frames per second) for

analysizing streaming velocity. For particle concentration experiments, TiO_2 nanoparticles with an average size of ~200 nm were dispersed into the liquid in a fairly uniform distribution.

References

[1] Sire, C., Lepilliet, F. S., Seo, J. -W., Hersam, M. C., Dambrine, G., Happy, H.& Derycke, V. Flexible Gigahertz Transistors Derived from Solution-Based Single-Layer Graphene. *Nano Lett.* **12,** 1184-1188 (2012).

[2] Sun, L., Qin, G. X., Huang, H., Zhou, H., Behdad, N., Zhou, W. D. & Ma, Z. Q. Flexible high-frequency microwave inductors and capacitors integrated on a polyethylene terephthalate substrate. *Appl. Phys. Lett*. **96,** 013509 (2010).

[3] Rogers, J. A., Someya, T., Huang &Y. G. Materials and Mechanics for Stretchable Electronics. *Science* **327,** 1603-1607 (2010).

[4] Park, S. I., Xiong, Y. J., Kim, R. H., Elvikis, P., Meitl, M., Kim, D. H., Wu, J., Yoon, J., Yu, C. J., Liu, Z. J., Huang, Y. G., Hwang, K., Ferreira, P., Li, X. L., Choquette, K. &Rogers, J. A. Printed Assemblies of Inorganic Light-Emitting Diodes for Deformable and Semitransparent Displays. *Science* **325,** 977-981 (2009).

[5] Ko, H. C., Stoykovich, M. P., Song, J. Z., Malyarchuk, V., Choi, W. M., Yu, C. J., Geddes, J. B., Xiao, J. L., Wang, S. D., Huang, Y. G. & Rogers, J. A. A hemispherical electronic eye camera based on compressible silicon optoelectronics. *Nature* **454,** 748-753 (2008).

[6] Kim, S., Jeong, H.Y., Kim, S. K., Choi, S. -Y. & Lee, K. J. Flexible Memristive Memory Array on Plastic Substrates. *Nano Lett.* **11,** 5438-5422 (2011).

[7] Liu, B., Zhang, J., Wang, X. F., Chen, G., Chen, D., Zhou, C. & Shen, G. Hierarchical Three-Dimensional ZnCo2O4 Nanowire Arrays/Carbon Cloth Anodes for a Novel Class of High-Performance Flexible Lithium-Ion Batteries. *Nano Lett.* **12**, 3005-3011 (2012).

[8] Xiao, S. Y., Che, L. F., Li, X. X.& Wang, Y. L. A novel fabrication process of MEMS devices on polyimide flexible substrates. *Microelectron. Eng.* **85,** 452-457 (2008).

[9] Lemke, T., Biancuzzi, G., Feth, H., Huber, J., Frank Goldschmidtböing, F. & Woias, P. Fabrication of normally-closed bidirectional micropumps in silicon-polymer technology featuring photopatternable silicone valve lips. *Sens. Actuator A-Phys.* **168,** 213-222 (2011).

[10] Wright, R., Hakemi, G. & Kirby, P. Integration of thin film bulk acoustic resonators onto flexible liquid crystal polymer substrates. *Microelectron Eng.* **88,** 1006-1009 (2011).

[11] Akiyama, M., Morofuji, Y., Kamohara, T., Nishikubo, K., Tsubai, M., Fukuda, O.& Ueno, N. Flexible piezoelectric pressure sensors using oriented aluminum nitride thin films prepared on polyethylene terephthalate films. *J. Appl. Phys.* **100,** 114318 (2006).

[12] Geiger, E.J., Pisano, A. P. & Svec, F. J. A polymer-based microfluidic platform featuring on-chip actuated hydrogel valves for disposable applications. *J. Microelectromech. Syst.* **19,** 944-950 (2010).

[13] Fachberger, R. & Erlacher, A. Applications of wireless SAW sensing in the steel industry. *Procedia Eng.* **5**, 224-227 (2010).

[14] Lee, K., Wang, W., Kim, T. & Yang, S. A novel 440 MHz wireless SAW microsensor integrated with pressure--temperature sensors and ID tag. *J. Micromech. Microeng.* **17,** 515 (2007).

[15] Donohoe, B., Geraghty, D. & O'Donnell, G. E. Wireless Calibration of a Surface Acoustic Wave Resonator as a Strain Sensor. *IEEE Sensors J.* **11**,1026-1032 (2011).

[16] Joshi, S.G. Flow sensors based on surface acoustic waves. *Sens.& Actuat.* ***A*** **44**, 191-197(1994).

[17] Lim, C., Wang, W., Yang, S. &Lee, K. Development of SAW-based multi-gas sensor for simultaneous detection of CO_2 and NO_2 *Sens. Actuat. B* **154** , 9-16 (2011).

[18] Lee, D.S. Luo, J. K., Fu, Y.Q., Milne, W.I., Park, N.M., Kim, S.H., Jung, M.Y.& Maeng, S. A SAW device made by using piezoelectric ZnO thin film layer on silicon wafer and its application to mixing in the droplet, *J. Nanosci. Nanotech.* **9**, 4626-4629 (2008).

[19] Fu, Y. Q., Luo, J. K., Du, X. Y., Flewitt, A. J., Li, Y., Markx, G. H., Walton, A. J. & Milne, W. I. *Sens. Actuat. B* **143**, 606-619 (2010).

[20] Du, X.Y., Fu, Y. Q., Tan, S. C., Luo, J. K., Flewitt, A. J., Milne, W. I., Lee, D. S., Park, J. Park, N. M. & Choi, Y. J. ZnO film thickness effect on surface acoustic wave modes and acoustic streaming. *Appl. Phys. Lett.* **93,** 094105 (2008).

[21] Fu, Y.Q., Garcia-Gancedo, L., Pang, H. F., Porro, S., Gu, Y. W., Luo, J. K., Zu, X. T., Placido, F., Wilson, J. I.B. & Flewitt, A. J. Microfluidics based on ZnO/nanocrystalline diamond surface acoustic wave devices. *Biomicrofluidics* **6**, 024105 (2012).

[22] Luo, J. K., Fu Y. Q., Ashley, G. &Milne, W.I. Integrated ZnO film based acoustic wave microfluidics and biosensors. *Adv. Sci. Technol.* **67**, 49-58 (2010).

[23] Wiklund, M., Günther, C., Lemor, R., Jäger, M., Fuhr, G. & Hertz, H.M. Ultrasonic standing wave manipulation technology integrated into a dielectrophoretic chip. *Lab Chip* **6**, 1537-1544 (2006).

[24] Guttenberg, Z., Muller, H., Habermüller, H., Geisbauer, A., Pipper, J., Felbel, J.,Kielpinski, M., Scriba, J. & Wixforth, A. Planar chip device for PCR and hybridization with surface acoustic wave pump. *Lab Chip* **5**, 308-317 (2005).

[25] Matsumura, M. & Camata, R.P., Pulsed laser deposition and photoluminescence measurements of ZnO thin films on flexible polyimide substrates. *Thin Solid Films* **476**, 317-321 (2005).

[26] Lee, C., Park, C., Cho, Y., Park, M., Lee, W. I. & Kim, H. W. Influence of ZnO buffer layer thickness on the electrical and optical properties of indium zinc oxide thin films deposited on PET substrates. *Ceram. Int.* **34**, 1093-1096 (2008).

[27] Datasheet of Dupont Kapton, http: //www2.dupont.com/Kapton/en_US/ assets/downloads/ pdf/summaryofprop.pdf, (2006)

[28] Ievtushenko, A. I., Karpyna,V. A., Lazorenko V. I., Lashkarev, G. V., Khranovskyy, V. D., Baturin, V. A., Karpenko, O. Y. , Lunika, M. M., Avramenko, K. A. & Strelchuk, V. V., High quality ZnO films deposited by radio-frequency magnetron sputtering using layer by layer growth method. *Thin Solid Films* **518**, 4529-4532 (2010).

[29] Lim, W.T., Lee, C. H. ,Highly oriented ZnO thin films deposited on Ru/Si substrate. *Thin Solid Films* **353**, 12-15 (1999).

[30]Tripathi, R., Kumar, A., Bharti, C., Sinha, T. P., Dielectric relaxation of ZnO nanostructure synthesiz ed by soft chemical method, *Current Appl. Phys.* **10**, 676-681 (2010)

[31] Wei, C. L. , Chen, Y. C. , Cheng, C. C. , Kao, K. S., Cheng, D. L. & Cheng, P. S. Highly sensitive ultraviolet detector using a ZnO/Si layered SAW oscillator. *Thin Solid films* **518**, 3059-3062 (2010)

[32]Suchea, M., Christoulakis, S., Moschovis, K., Katsarakis, N., Kiriakidis, G., ZnO transparent thin films for gas sensor applications. *Thin Solid Films* **515**, 551-554 (2006)

[33] Phan, D. T. & Chung, G. S., The effect of post-annealing on surface acoustic wave devices based on ZnO thin films prepared by magnetron sputtering, Appl. Surf. Sci. **257**, 4339-343 (2011)

[34] Achenbach, J. D. and Keshava, S. P.,Free wave in a plate supported by a semi-infinite continuum, *J. Appl. Mech.* **34**, 397-404 (1967)

[35] Auld, B. A., *Acoustic Fields and Waves in Solids* (Wiley, New York, 1973).

[36] Oh, H., Wang, W., Lee, K., Park, I. & Yang, S. S. Sensitivity improvement of wireless pressure sensor by incorporating a SAW reflective delay line. *Int. J. on Smart Sensing & Intelligent Syst.* **1 ,** 940-954 (2008).

[37] Du, X. Y., Swanwick, M. E., Fu, Y. Q., Luo, J. K., Flewitt, A. J., Lee, D. S., Maeng, S.& Milne, W. I. Surface acoustic wave induced streaming and pumping in 128° Y-cut LiNbO3 for microfluidic applications. *J. Micromech. Microeng.* **19**, 035016 (2009).

[38] Brizoual, L.L., Sarry, F., Elmazria, O., Alnot, P., Ballandras, S. & Pastureaud, T. GHz Frequency ZnO/Si SAW Device. *IEEE Tran. Ultrason. Ferroelectr.Freq.Control.* **55**, 442-450 (2008).

[39] Zhang, A. L., Wu, Z. Q. &Xia, X. H. Transportation and mixing of droplets by surface acoustic wave. *Talanta* **84**, 293-297 (2011).

[40] Alghane, M., Chen, B. X., Fu, Y. Q., Li, Y., Luo, J. K. & Walton, A. J. Experimental and numerical investigation of acoustic streaming excited by using a surface acoustic wave device on a 128° YX-$LiNbO_3$ substrate. *J. Micromech. Microeng.* **21**, 015005 (2010).

[41] Shi, J., Ahmed, D., Mao, X., Lin, S. C. S., Lawit, A. &Huang, T. J. *Lab Chip*. **9**, 2890-2895 (2009).

Acknowledgements: This work was supported by the National Natural Science Foundation Key Program of China (No. 60936002), the National Natural Science Foundation of China (Nos. 61171038, 61006077, 61204124 and 61274123), the Research Fund of International Young Scientists (No. 61150110485), the Zhejiang Province Natural Science Fund key Project (No. J20110271), and the Zhejiang Provincial Natural Science Foundation (No. LQ12F01007, LR12F04001, and Z1110168). The authors thank the Innovation Platform for Micro/Nano Device and System Integration at Zhejiang University.

Author contributions

Zhou J, He X.L, Wang W.B. deposited and characterized ZnO thin films, fabricated SAW devices and conducted sensing and microfluidics experiments. Zhou, He and Guo did the simulation and theoretical analysis. Jin H, Xu Y, Dong S R, Wang D M, Geng J, Luo J.K. and Milne W I supervised the project, analyzed the results and wrote the paper.

Competing financial interests: The authors declare no competing financial interests.

Figures and figure captions

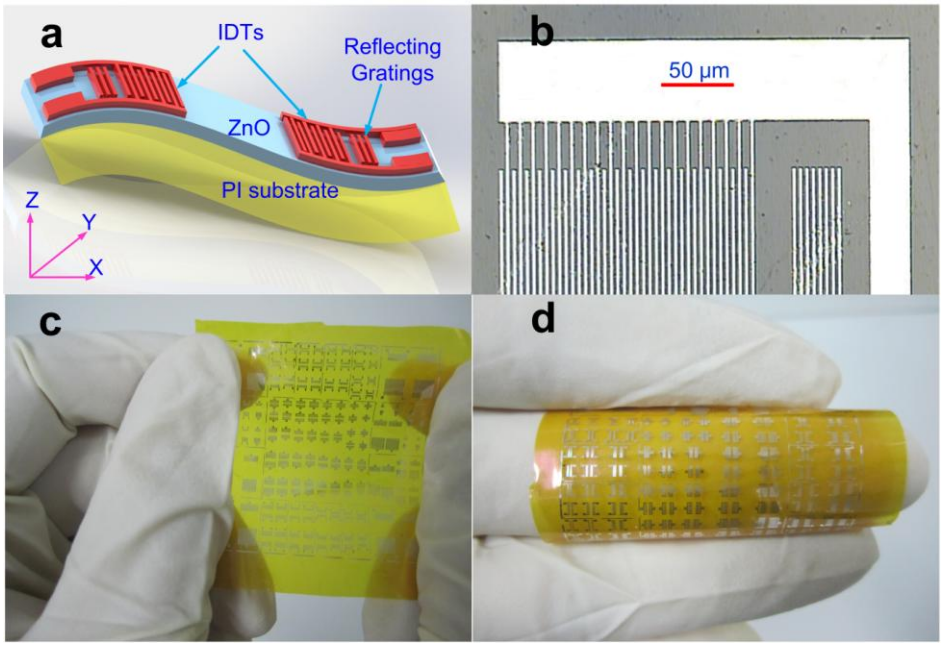

Figure 1. The flexible thin film ZnO/polyimide SAW devices: (a) Three-dimensional schematic of the developed SAW device on a ZnO/polymer substrate; (b) Microscope image of a SAW device with a 20 pairs of IDT figure; (c) & (d) Photographs of semi-transparent and flexible SAW devices on polyimide.

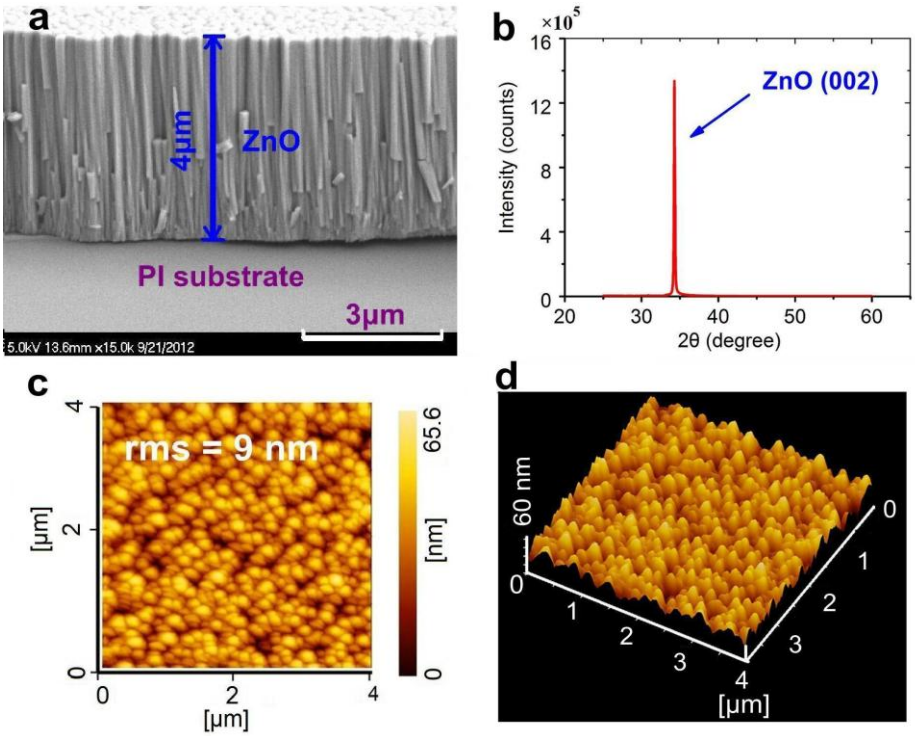

Figure 2. Characterization of ZnO thin film deposited on polyimide substrate. (a) An SEM image of the cross-section; (b) XRD pattern of the ZnO layer; (c) & (d) AFM images. The root mean square of the surface roughness is about 9 nm.

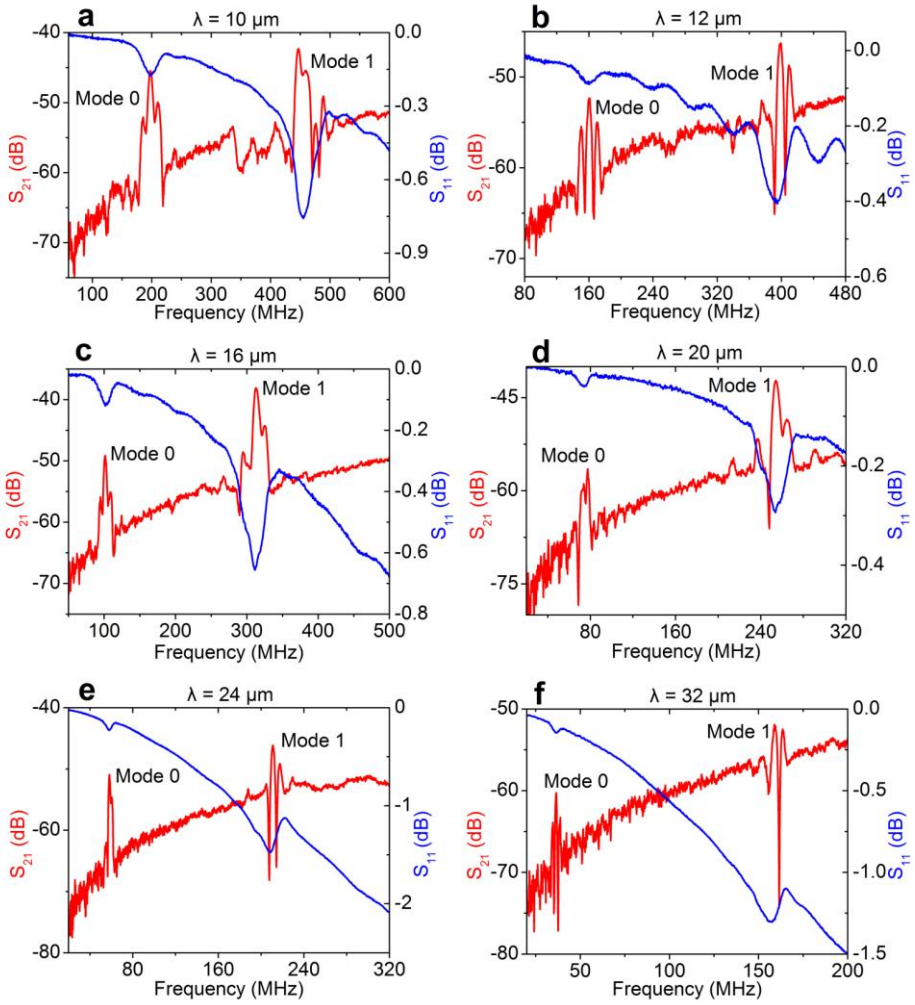

Figure 3. Transmission spectrum of the flexible ZnO/polyimide SAW devices with 4 μm thick ZnO film as a function of wavelength, λ, (a) λ =10 μm; (b) 12 μm; (c) 16 μm; (d) 20 μm; (e) 24 μm and (f) 32 μm. Two well-defined resonant modes with high amplitude were obtained from all devices with different wavelengths. All the SAW devices have 20 pairs of IDT fingers.

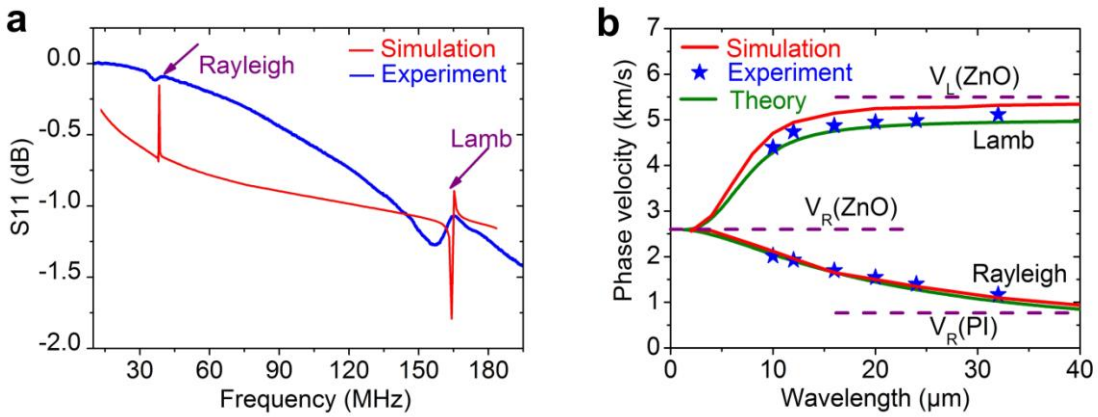

Figure 4. The experimental and simulation spectra (a) and phase velocity (b) of the flexible ZnO/polyimide SAW devices with a 4 μm thick ZnO thin film as a function of wavelength. The wavelength used for simulating the spectrum in (a) is 32 μm. The two well defined resonant peaks are in good agreement with the experimental result. The phase velocity of the Rayleigh wave decreases and approaches that in the polymer substrate, while that of the Lamb wave approaches that in the ZnO layer as the wavelength increases. The SAW devices have 20 pairs of IDT fingers.

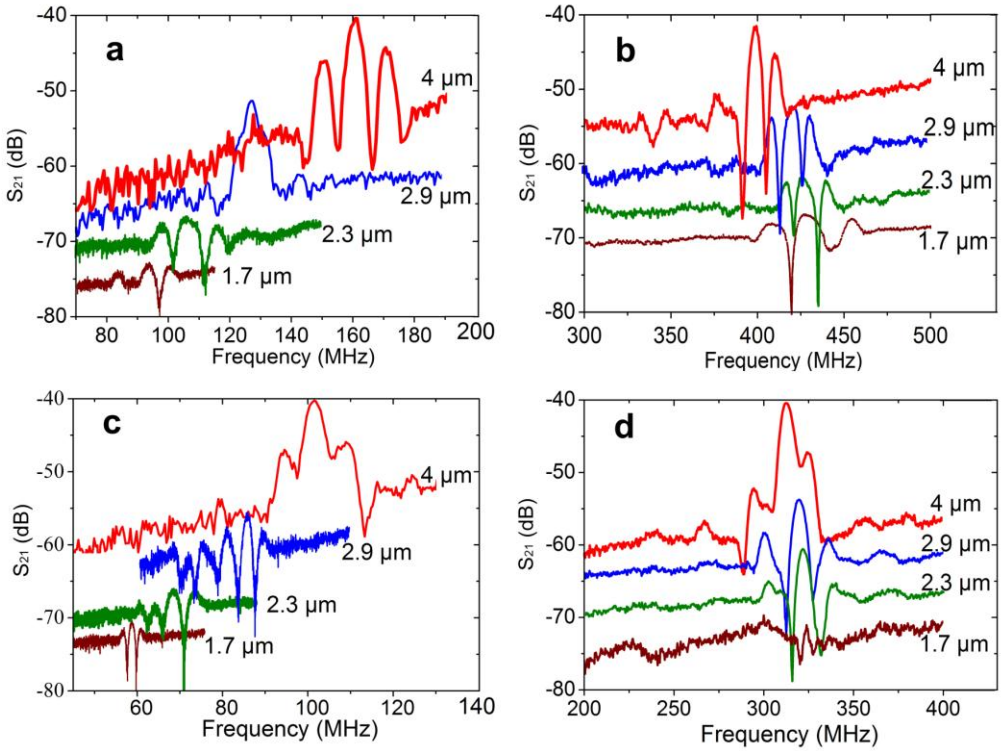

Figure 5. The effect of the thickness of ZnO film on the resonant responses of the Rayleigh wave and the Lamb wave of the flexible Al/ZnO/polyimide SAW devices with a wavelength of 12 μm for (a) the Rayleigh wave, and (b) the Lamb wave; A wavelength of 16 μm was used for (c) the Rayleigh wave, and (d) the Lamb wave. The SAW devices have 20 pairs of IDT fingers. (the different spectra are presented on top of each other for clarity)

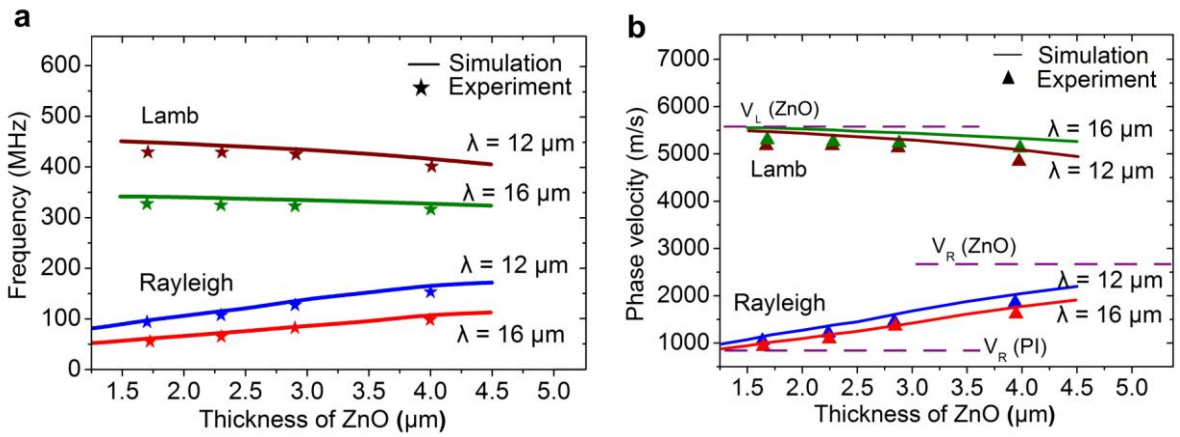

Figure 6. Comparison of experiments and FEA simulation results on the resonant frequency and phase velocity vs. thickness of ZnO film at different wavelengths. The lines are obtained from simulation, whereas the symbols are the experimental data. The SAW devices have 20 pairs of IDT fingers.

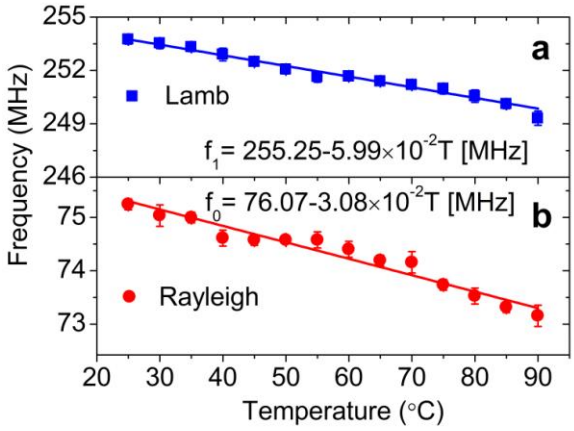

Figure 7. Resonant frequency as a function of temperature for the zero mode wave (a) and the first mode wave (b). The resonant frequencies decrease linearly with increase of the temperature showing a TCF of 442 and 245 ppm/K for the zero and first mode wave respectively. The SAW devices have a wavelength of 20 μm and 20 pairs of IDT fingers.

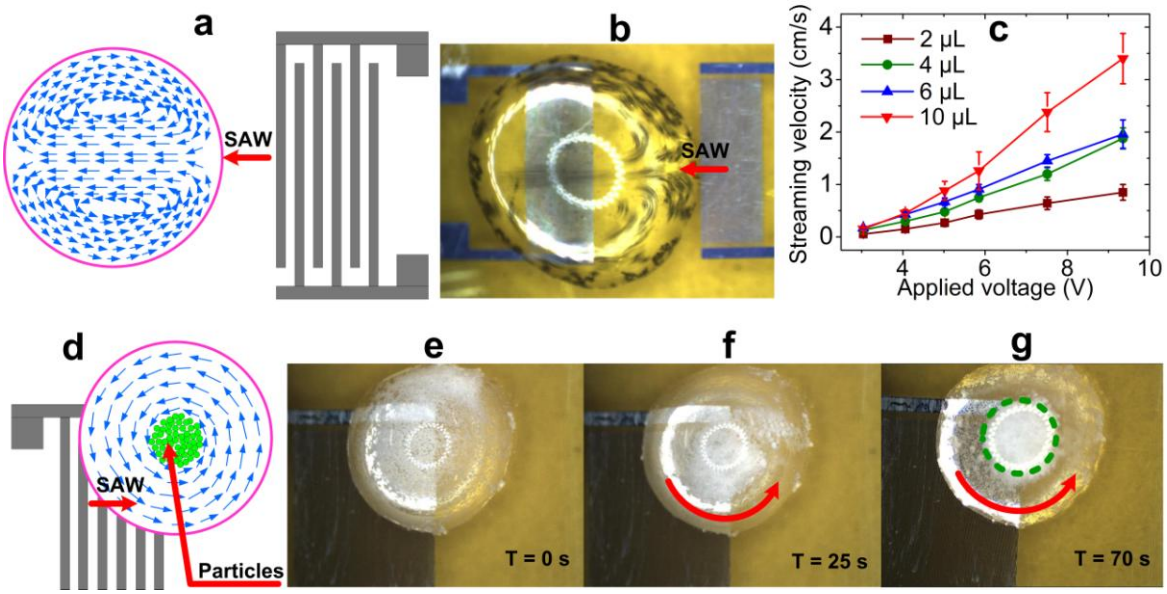

Figure 8. (a) A schematic drawing of acoustic streaming inside a liquid droplet, (b) a snapshot of acoustic streaming induced by the flexible SAW device, showing a double vortex streaming pattern. (c) Streaming velocity as a function of RF signal voltage with droplet size as a parameter, showing a linear increase in streaming velocity with signal voltage. (d) A schematic drawing to show circulating streaming and particle concentration induced by SAW off the central wave path. Particles are uniformally distributed in liquid (e) and partial concentration in the droplet after applying a RF signal for 25 sec (f) and 70 sec (g) with a signal voltage of 25 V. The SAW device used for these experiments has 50 pairs of IDT fingers, and a wavelength of 12 μm. Only the Rayleigh Wave was used for microfluidic experiments. The red curved arrows are indicative of the streaming direction, and the green circle shows the area with the highly concentrated nanoparticles.

Supplementary Information

Flexible surface acoustic wave resonators built on disposable plastic film for electronics and lab-on-a-chip applications

Hao Jin, Jian Zhou, Xingli He, Wenbo Wang, Hongwei Guo, Shurong Dong, Demiao Wang, Yang Xu, J.K. Luo, Junfeng Geng and W.I.Milne

1. **The mean crystallite grain size**, D, was estimated using the Debye–Scherrer formula[30] as 72.3 nm from

$$D = K\lambda/(\beta cos\theta) \quad \text{(S1)}$$

where K is the shape factor of the average crystallite with a value of 0.94, λ the X-ray wavelength (1.5405 Å for Cu target), β the FWHM in radians, θ the Bragg angle. The mean grain size is about 72.3 nm for a 4 μm thick ZnO film, comparable to or larger than most of the ZnO previously deposited on solid substrates.

2. Tables.

Table S1. The effect of the wavelength on the characteristics of flexible SAW devices with a 4 μm thick ZnO film.

sample no.	λ (μm)	f_0 (MHz)	v_{p0} (ms^{-1})	f_1 (MHz)	v_{p1} (ms^{-1})
A1	10	198.1	1981	447	4470
A2	12	161	1932	399.2	4790.4
A3	16	101.5	1624	313.1	5009.6
A4	20	75	1500	253	5060
A5	24	56.4	1353.6	211.1	5066.4
A6	32	34.4	1100.8	158.5	5072

Table S2. The effect of ZnO film thickness on the characteristics of the flexible SAW devices with different wavelengths.

Sample	λ (μm)	ZnO (μm)	f_0 (MHz)	v_{p0} (ms^{-1})	f_1 (MHz)	v_{p1} (ms^{-1})
B1	16	1.7	58.6	937.6	323.9	5182.4
B2		2.3	68.5	1096	321.2	5139.2
B3		2.9	85.5	1368	319.6	5113.6
B4		4	101.5	1624	313.1	5009.6
C1	12	1.7	93.5	1122	427	5124
C2		2.3	107	1284	426.8	5121.6
C3		2.9	127	1524	423.1	5077.2
C4		4	161	1932	399.2	4790.4

3. The phase velocity of the polyimide. It can be estimated from the following equation,

$$v_p = 0.93\sqrt{E/2(1+\sigma)\rho_0} \quad \text{(S2)}$$

where E is the Young' modulus, σ the Poisson's ratio and ρ_0 the density of materials. The polyimide has a Young's modulus E of 2.5 GPa, σ of 0.34, and ρ_0 of 1.42×103 kg/m^3 (from the datasheet of Dupont Kapton® 100H). The theoretical Rayleigh wave velocity of the polyimide substrate is thus 754 m/s, much smaller than that in ZnO. The thickness, Young's modulus, Poisson's ratio and density of the Al electrode were set to be 100 nm, 70 GPa, 0.35 and 2.7 g/cm^3, respectively, while the material constants of the ZnO were taken from Ref. 38.

4. SAW device modeling. Finite element analysis was used to model the transmission characteristics of the layered structure SAW devices using COMSOL Multiphysics software. For the modeling, the actual layer thicknesses and material properties of the polyimide (taken from the maker's data sheet), the ZnO layer (taken from Ref. 38), and the Al layer related data (The Young's modulus, Poisson's ratio and density are set to be 70 GPa, 0.35 and 2.7 g/cm^3) were used to model the phase velocities and resonant frequencies of the Al/ZnO/Polyimide SAW devices.

5. Theoretical analysis. To theoretically analyze the Rayleigh and Lamb waves propagated in a ZnO thin film on a PI substrate, the schematic structure and the coordinate system are shown in figure S1, where the ZnO is a thin layer and the polyimide is taken as an isotropic half space considering its thickness is much larger than the ZnO layer. The contact boundary condition between them is assumed to be welded.

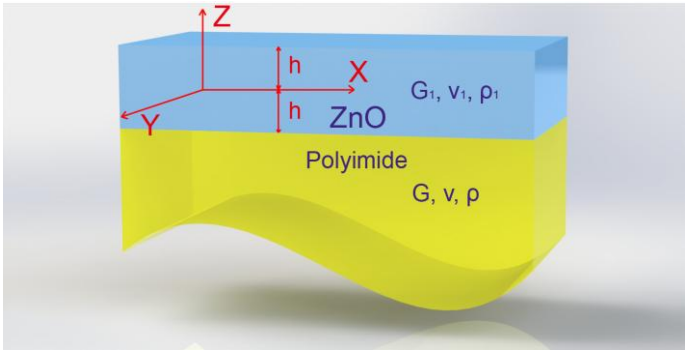

Figure S1. Schematic of an ZnO thin film on PI substrate for theoretical model analysis of Rayleigh and Lamb waves.

The displacement components in the x and z directions are denoted as u and w, respectively, whereas the displacement in the y direction vanishes for this condition. Assuming the thickness of ZnO is $2h$, the general displacements in the ZnO layer can be written as

$$u_1 = [A_1 e^{-kq_1 z} + B_1 e^{-kq_1 z}]e^{ik(x-ct)} - [C_1 e^{-ks_1 z} - D_1 e^{-ks_1 z}]e^{ik(x-ct)} \quad \text{(S3)}$$

$$w_1 = iq[A_1 e^{-kq_1 z} - B_1 e^{-kq_1 z}]e^{ik(x-ct)} - (i/s_1)[C_1 e^{-ks_1 z} + D_1 e^{-ks_1 z}]e^{ik(x-ct)} \quad \text{(S4)}$$

where k is the wave vector and c is the phase velocity, and A_1, B_1, C_1, D_1 are the unknowns to be determined. Intermediate variables q_1 and s_1 are defined as

$$q_1 = (1 - \alpha^2 \frac{\theta}{\gamma}\beta^2)^{1/2},$$

$$s_1 = (1 - \frac{\theta}{\gamma}\beta^2)^{1/2},$$

where $\beta = c/c_T$, $\theta = \rho_1/\rho$, $\gamma = G_1/G$, $\alpha_1^2 = (1-2v_1)/2(1-v_1)$, and c_T is the transverse wave velocity of the material. In the above equations, subscript "1" is used to distinguish the ZnO layer from the polyimide substrate, for which no subscript is used.

The general displacements in the polyimide substrate can be also written as

$$u = [Be^{kq(z+h)} + De^{ks(z+h)}]e^{ik(x-ct)} \quad \text{(S5)}$$

$$w = -i[qBe^{kq(z+h)} + (1+s)De^{ks(z+h)}]e^{ik(x-ct)} \quad \text{(S6)}$$

wherein $s = (1-\beta^2)^{1/2}$, $q = (1-\alpha^2\beta^2)^{1/2}$, $\alpha^2 = (1-2v)/2(1-v)$, B and D are also the unknowns to be determined. By substituting the displacement solution of the top layer (Eqs. S3 and S4) and the bottom half space (Eqs. S5 and S6) into the following stress-strain relations,

$$\sigma_x = \frac{2G(1-v)}{1-2v}\frac{\partial u}{\partial x} + \frac{2Gv}{1-2v}\frac{\partial w}{\partial x}, \sigma_z = \frac{2G(1-v)}{1-2v}\frac{\partial w}{\partial z} + \frac{2Gv}{1-2v}\frac{\partial u}{\partial x}, \sigma_{xz} = G(\frac{\partial u}{\partial z} + \frac{\partial w}{\partial x})$$

where G and ν represent the shear modulus and Poisson's ratio, respectively, we can get the stress components of each part. Because of the welded contact boundary conditions, the stress and the displacement are continuous in the interface, which can be written as follows:

At $z=h$, $[\sigma_z]_1 = 0$ and $[\sigma_{zx}]_1 = 0$.

At z=-h, $[\sigma_z]_1 = \sigma_z$, $[\sigma_{zx}]_1 = \sigma_{zx}$, $u_1 = u$, and $w_1 = w$.

By substituting the displacement and stress solution to the boundary conditions, we get a set of six equations with six unknowns (A_1, B_1, C_1, D_1, B and D) for nontrivial solutions. The determinant of the coefficients matrix must be zero, which leads to the characteristic equation shown as Eq.S7, wherein $\xi = kh$ is the dimensionless wave vector. By numerically solving the transcendental equation in Eq.S7 with geometrical and material parameters of our fabricated SAW devices, we can obtain the dispersion relation. The phase velocity of the Rayleigh wave in the ZnO layer decreases and approaches that in the polymer substrate, while that of the Lamb wave approaches that in the ZnO layer as the wavelength increases. The theoretical and experimental results are also shown in figure 4b for comparison, showing good agreement for both the Rayleigh and Lamb waves. These also agree well with that obtained by finite elemental analysis as shown in figure 4b.

$$\begin{vmatrix} (1+s_1^2)e^{-\xi q_1} & (1+s_1^2)e^{\xi q_1} & -2e^{-\xi s_1} & 2e^{\xi s_1} & 0 & 0 \\ -2q_1e^{-\xi q_1} & 2q_1e^{\xi q_1} & (s_1+\frac{1}{s_1})e^{-\xi s_1} & (s_1+\frac{1}{s_1})e^{\xi s_1} & 0 & 0 \\ (1+s_1^2)e^{\xi q_1} & (1+s_1^2)e^{-\xi q_1} & -2e^{\xi s_1} & 2e^{-\xi s_1} & \frac{(1+s_1^2)}{\gamma} & \frac{2}{\gamma} \\ -2q_1e^{\xi q_1} & 2q_1e^{-\xi q_1} & (s_1+\frac{1}{s_1})e^{\xi s_1} & (s_1+\frac{1}{s_1})e^{-\xi s_1} & \frac{2q}{\gamma} & \frac{(s+\frac{1}{s})}{\gamma} \\ e^{\xi q_1} & e^{-\xi q_1} & -e^{-\xi s_1} & e^{\xi s_1} & 1 & 1 \\ q_1e^{\xi q_1} & -q_1e^{-\xi q_1} & -\frac{1}{s_1}e^{\xi s_1} & -\frac{1}{s_1}e^{-\xi s_1} & -q & -\frac{1}{S} \end{vmatrix} = 0 \quad \text{(S7)}$$

6. The electromechanical coupling coefficient, K^2, is an important parameter to assess SAW devices. According to the equivalent circuit of a SAW transducer, it can be evaluated using

$$K^2 = \frac{\pi G_m(f_0)}{4NB_s(f_0)} \quad \text{(S8)}$$

where N is the finger pairs, $G_m(f_0)$ and $B_s(f_0)$ the motional conductance and static susceptance of the input port at f_0, respectively. A K^2 value of 1.05 % was obtained for the Rayleigh wave with f_0 = 198.1 MHz, and 0.8 % for the Lamb wave with f_1 = 447 MHz for Device A1. These

values are smaller than those obtained from SAW on ZnO on solid substrates, implying a high attenuation coefficient from the polymer substrates. The small K^2 values are believed to be associated with the slow streaming velocities observed. However it should be pointed out that for most lab-on-a-chip applications, a flow velocity up to one millimeter per second is more than sufficient. Therefore the results have clearly demonstrated that the flexible SAW properties are sufficient for applications in microfluidics and lab-on-a-chip. Furthermore, the signal amplitude up to 18 dB for both the zero and first mode waves is also sufficient for communication applications.